Magnetic Resonance in Medicine 41:1023–1031 (1999)

Flow Distortion and Signal Loss in Spiral Imaging

P.D. Gatehouse* and D.N. Firmin

The effect of in-plane motion on the point spread function (velocity PSF) in spiral imaging is studied experimentally and derived mathematically and is shown to consist of a smoothed, trailing edge and fringes around the leading edge. The velocity PSF remains largely in phase with the static PSF, consistent with the absence of signal loss by motion-related phase shifts in central *k* space. However, single-shot spiral imaging gives no clear improvement in complex and turbulent flow signal uniformity compared with echo-planar imaging with early, central *k*-space acquisition, which requires explanation given the spiral's earlier coverage of central *k* space. Alternate leading-edge fringes of the spiral's velocity PSF are in antiphase to the source, and cancellation may occur when these overlap other in-phase signals. Phase variations toward peripheral *k* space in turbulent flow also cause distortion. It is concluded that spiral imaging may lose complex and turbulent flow signals because of complex PSF distortion. Magn Reson Med 41:1023–1031, 1999. © **1999 Wiley-Liss, Inc.**

Key words: spiral; echo planar; flow; motion; point spread; function

This investigation was motivated by the observation of motion and flow artefacts in spiral imaging. The effect of in-plane motion on the point spread function (velocity PSF) in spiral imaging is studied in experiments and in computer simulations, and a simplified mathematical model is derived on the basis of the previously published velocity *k*-space analysis (1). Signal loss in spiral imaging of complex and turbulent flows also is studied by comparison against single-shot echo-planar imaging (EPI), and an explanation is proposed.

Spiral Imaging

In spiral imaging (2–4), the nuclear magnetic resonance (NMR) signal is acquired during traversal of a spiral path in *k* space. Off-resonance errors distort the spiral path and cause artefacts (5), which can be corrected in part (6–8). Single-shot spiral imaging is made more practicable by using real-time imaging for the interactive adjustment of shimming and tuning controls (9). A high priority in designing spiral imaging gradient waveforms is to reduce off-resonance sensitivity by acquiring the data as rapidly as possible rather than obtaining a uniform sampling density over *k* space (10,11).

Spiral In-Plane Flow Effects

In-plane flow effects have been assumed to be minimal because of the early acquisition of central *k* space and the periodic return through zero of all orders of motion-related phase shift of the spiral gradient wave forms (12), which nearly coincide with the spatial phase shift (in the same direction) returning to zero. Although the reduction of intravoxel, phase-dispersive signal loss by early central *k*-space acquisition is clear, some distortion was shown in a simulated PSF of a source moving during a spiral scan (13). This distortion occurred in images of in-plane flow and was explained as a misregistration of spatial frequency data (9). The velocity phase shift plotted over *k* space (1) showed the velocity phase curvature occurring mainly in the direction of motion, and this curvature forms the basis for the theoretical derivation of the effect of velocity on the PSF in the Discussion.

PSF Distortion by Motion in Conventional Imaging

The PSF of a static point source is affected by factors such as the finite *k*-space coverage of the imaging sequences. When the point source is moving, its motion causes further distortion, which is called the ''velocity PSF'' in this paper. The final image of the moving point source is given by the convolution of the static PSF with the velocity PSF. The velocity PSF due to motion along a readout gradient of constant amplitude (14,15) will be relevant in the Discussion. It is small in conventional magnetic resonance imaging (MRI), but it is more severe as ''segmented chirp'' in EPI. The velocity PSF is a quadratic phase curvature across x at a constant amplitude, as discussed previously (15). The increasing phase slope may be interpreted as causing an intravoxel phase cancellation beyond a certain distance to either side of the centre of $P(x)$, dependent upon the phase curvature in $P(x)$, and also the static PSF of the point source due to other factors, such as the finite extent of sampling in *k* space. The quadratic phase curvature in $P(x)$ is inversely proportional to the phase curvature across the raw data, and therefore reduces with increasing velocity, so that, for a given pixel size, the width of the velocity PSF increases with velocity. The behaviour of the velocity PSF as $v \rightarrow 0$ should be considered, because its amplitude $\rightarrow \infty$, although this is accompanied by an infinitely large phase slope when $x \neq 0$, and with a finite pixel width $P(x)$, might be regarded as $\delta(x)$.

MATERIALS AND METHODS

MRI Scanner Apparatus

A 0.5 T whole-body scanner was used with pulse-sequence generation and data acquisition by a Surrey Medical Imaging Systems console (Guildford, UK). A whole-body gradient system capable of 13 mT/m in 400 μsec rise time enabled single-shot imaging.

Magnetic Resonance Unit, Royal Brompton Hospital, London, United Kingdom.
*Correspondence to: P.D. Gatehouse, Magnetic Resonance Unit, Royal Brompton Hospital, Sydney Street, Chelsea, London SW3 6NN, United Kingdom. E-mail: p.gatehouse@rbh.nthames.nhs.uk
Received 4 February 1998; revised 11 November 1998; accepted 26 December 1998.

Pulse Sequences

Single-Shot Spiral

A gradient-echo 32-cycle, single-shot, constant slew rate, spiral-imaging sequence was implemented (Table 1) with velocity-compensated slice selection. For reconstruction, the complex raw data was regridded before two-dimensional fast Fourier transform (2D-FFT) (16).

Interleaved Spiral Imaging

An interleaved, spiral-imaging sequence with velocity-compensated slice selection acquired images with 192 pixels over 384 mm FOV in six 31.40 msec or 16 11.9 msec interleaved readouts, which started as constant slew-rate and changed to constant amplitude on reaching the peak gradient amplitude (12). Images were reconstructed by using the same method that was used for the single-shot spirals.

Single-Shot EPI

Single-shot EPI was used as a reference level for the amount of signal loss in complex and turbulent flows. Three versions of single-shot EPI were used, with the coverage of central *k* space at echo numbers 32, 16, and 8 (where 1 = the first, odd, gradient echo of the 64 in the phase-encode FFT direction), with phase-encode velocity compensation at central *k* space, and with velocity-compensated slice selection. A conventional EPI reconstruction method of reversing alternate echoes before 2D-FFT was used, with forward and reversed echoes aligned to null Nyquist ghosting of static material. The sampling bandwidth was 200 kHz at a readout gradient strength of 9.40 mT/m for an FOV of 500 mm, using 350 μsec constant sections with 250 μsec sinusoidal ramps.

Spiral Imaging of In-Plane Constant Velocity Phantom

An approximation to the velocity PSF was imaged by using a 20 mm diameter solid object moving at a constant 1.9 m/second velocity. The image of a moving object is a superposition of moving point sources, which, in practice, may have slightly different PSFs due to main field inhomogeneity, eddy current effects, etc. Phase shifts in the velocity-related PSF also may cause the imaged linear superposition of points to differ from that of a single point source image.

Table 1
Parameters of Single-Shot Spiral Gradient Waveforms

Measure	Constant angular rate	Constant slew rate	Constant *k*-space speed
Cycles	32	32	32
Resolution (mm)	4	4	4
Field of view (FOV) diameter (mm)	256	256	256
Duration (msec)	54.4	36.37	19.75
Peak g (mT/m)	10.8	12	15
Peak slew (mT/m/msec)	40	40	775

Single-Shot Imaging of Complex and Turbulent Flows

The reduction of signal loss in EPI with earlier central *k*-space coverage was used as a reference for comparison against the spiral imaging. The single-shot spiral sequence was compared against single-shot EPI in two flow phantoms. In the first phantom, the fluid was carried into a cylinder with a diameter of 8 cm and a length of 25 cm by a 1.27 cm inner diameter (ID) tube at about 1 m/second entering obliquely through the side wall near one end of the cylinder; and flow left the cylinder through the centre of the other end. The tangential component of the entry velocity established a complex circulating flow in the cylinder. The cylinder was placed parallel to the *z*-axis (magnet bore axis), and transverse images were obtained. The second experiment used a turbulent flow downstream of an abrupt 5 mm stenosis in a 24 mm ID tube at 130 cm^3/second flow rate. The tube containing the stenosis was placed parallel to the *z*-axis, and sagittal images were obtained.

Computer-Simulated Images and Point-Spread Functions

The computer simulations used gradient waveforms recorded from each pulse program. Simulated data from 25 spin isochromats (“spins”) were used to model the PSF phantom, all moving with the same velocity, and were distributed in a 5×5 matrix of image pixels. The complex sum of the spins’ signals was reconstructed by using the same procedures that were used for genuine image data. For velocity *k*-space analysis, the phase of the centre spin of the simulated group was taken as a function of (k_x, k_y) by using the image reconstruction procedure to reorganise the raw data into a 2D *k*-space matrix, but with no FFTs. No relaxation decay effects were programmed. The simulations of complex flow used the computed signal from a group of up to 1600 spins with specified positions and velocities.

RESULTS

Spiral Imaging of Moving Point Source

The solid moving object experiments and simulations (Fig. 1) demonstrated an in-plane motion artefact. The trailing edge of the moving object becomes blurred, and a series of fringes appears off its leading edge.

Interleaved spiral images of the in-plane descending aorta generally show even the fastest moving blood without flow artefacts. However, in a cardiac short-axis oblique plane, a small volume or “plug” of blood in the aorta was excited and imaged as it moved obliquely out of and across the excitation plane, and the in-plane motion caused a semicircular fringe at its leading edge (17), consistent with the effects in phantom imaging. No offset or asymmetric distortion was observed in the image plane direction *perpendicular* to the direction of motion.

Single-Shot Imaging of Complex and Turbulent Flows

The images of complex flow (Fig. 2) show that the amount of signal loss in the spiral image (Fig. 2d) is approximately similar to that in the single-shot EPI using echo 16 at central *k* space (Fig. 2b). The images of turbulent flow

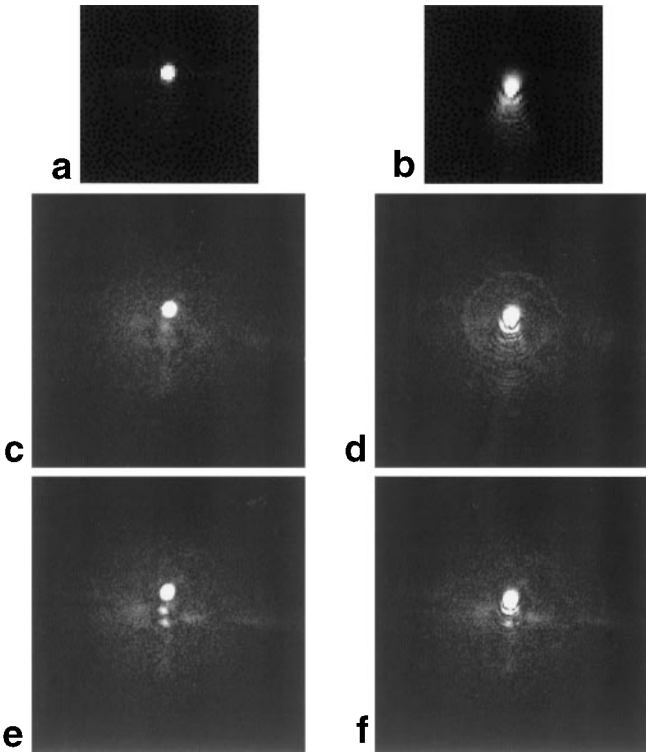

FIG. 1. Point-spread function (PSF) phantom single-shot and interleaved spiral images of in-plane velocity. Images in the left column show the phantom stationary at the position that triggered the scan through the optical sensor. Images in the right column show the phantom moving at 1.9 m/second down the page. **a,b:** Single-shot spiral. **c,d:** Six-interleaf spiral. **e,f:** Sixteen-interleaf spiral. The two smaller objects below the phantom in e are signals from plastic in the mechanism that moved the phantom.

(Fig. 3) show that the signal loss in the spiral image (Fig. 3d) approximately resembles the loss in the single-shot EPI using echo 16 at central *k* space (Fig. 3b).

DISCUSSION

Spiral Imaging In-Plane Motion Artefact

The in-plane motion artefact results from the misregistration of the spatial frequencies forming the small point source. The low spatial frequencies are acquired early in the spiral readout, and they add to represent the object near its starting position. The higher spatial frequencies are acquired late in the readout, and they add to represent the object near its position at the end of the readout. The smoothed trailing edge and the fringes around the leading edge of the object are the result. Similar distortion of flow across the axis of a 2D-selective radiofrequency (RF) pulse using a spiral *k*-space path has been observed (18,19) and also may be explained on the basis of this work. The distortion may be derived mathematically by using the velocity *k*-space plots and the velocity-related PSFs obtained by taking 2D-FFTs of velocity *k* space (Fig. 4). The phase curvature along the k_x axis causes increasing misregistration of the higher spatial frequencies. Across a conventional gradient-echo readout, the velocity phase slope through negative k_x opposes that through positive k_x; now, in spiral imaging *both* negative and positive k_x have the *same* phase slope. This might be expected to introduce asymmetry to the velocity-related PSF.

The three forms of spiral path shown in Figure 4 show similar phase curvatures, although the peak phase is reduced because of the faster coverage by the constant slew rate and constant *k*-space speed spirals. Considering the velocity phase shift as a function of time during a spiral readout, the oscillating velocity phase shift is expected to increase as the amplitude of the gradient waveforms increases and also as their frequency of oscillation slows down. Comparing the constant angular rate spiral against the constant slew-rate spiral gradient waveforms, the gradient waveform amplitude increases less rapidly as the frequency of oscillation falls. For the constant *k*-space speed spiral, the gradient amplitude is constant, and the

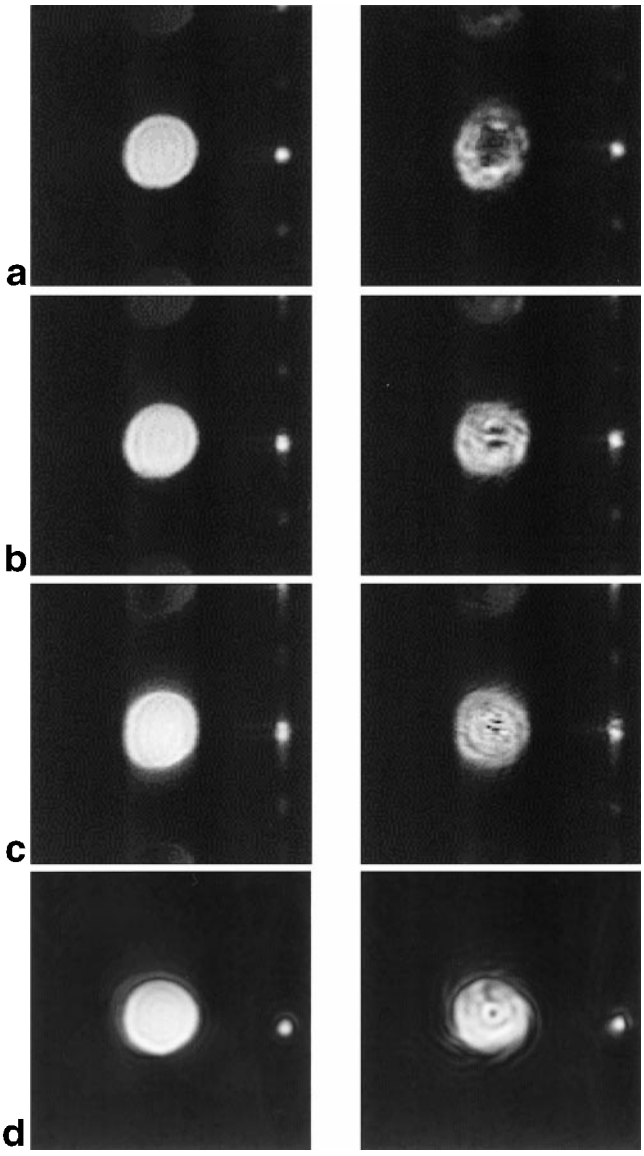

FIG. 2. Single-shot imaging of complex flow. The echo-planar imaging (EPI) and spiral data were reconstructed into 256-pixel images by using zero filling before 256-point fast Fourier transforms (FFTs). Images with flow off are shown in the left column for each method. **a–c:** Single-shot EPI with central *k* space at echo 32 (a), 16 (b), and 8 (c) of the 64. **d:** Single-shot spiral imaging.

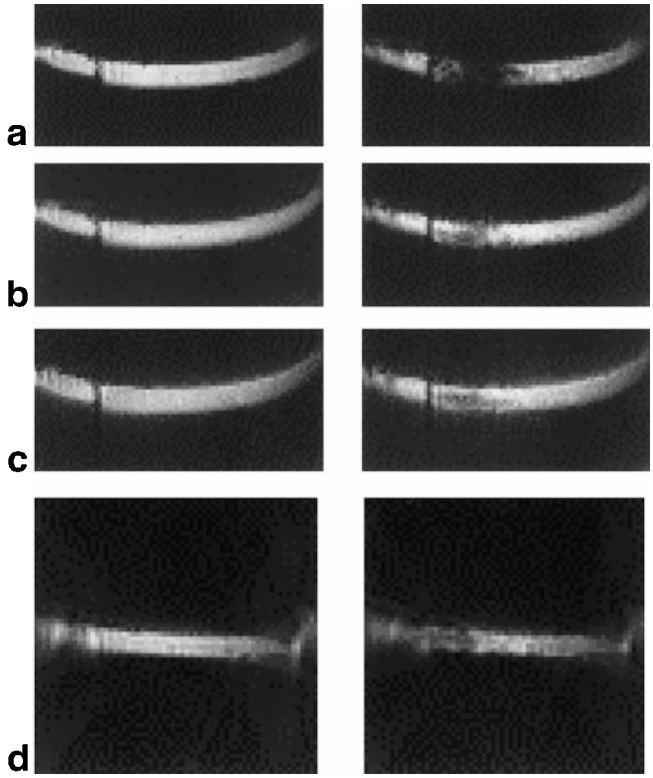

FIG. 3. Single-shot imaging of turbulent flow. Images with flow off are show in the left column for each method. **a–c:** Single-shot EPI with central *k* space at echo 32 (a), 16 (b), and 8 (c) of the 64. **d:** Single-shot spiral imaging. Each experiment was repeated ten times to determine the average level of signal loss.

increasing amplitude of the oscillating phase shift comes entirely from the fall in the oscillation frequency.

By adapting the derivation of readout motion PSF distortion, an approximation to the observed in-plane motion spiral velocity PSF may be obtained. The phase variation across velocity *k* space on the k_x axis will be approximated by a quadratic phase curvature, $V(t)$, which changes sign at $t = 0$:

$$V(t) = (1 - H(t)) \exp(-i2\pi Gvt^2/2) + H(t) \exp(i2\pi Gvt^2/2), \quad [1]$$

where the readout gradient amplitude $G = \gamma g$, v = velocity along readout gradient G, and $H(t)$ is the Heaviside unit step function, which = 0 for $t < 0$ and = 1 for $t > 0$. Equation 1 takes no account of the different velocity-related phase curvature along other radial directions in *k* space but will show how the spiral velocity-related PSF is so asymmetric compared with that of the conventional gradient-echo readout. The line $V(t)$ across the raw data therefore is modelled as a projection readout across *k* space in the constant gradient G lasting from $-t_s$ to $+t_s$, but with a quadratic phase curvature that changes sign at $t = 0$. The phase curvature is identical to the raw data from a point source moving during the readout gradient, toward the centre of the image from $x = vt_s$ at time $t = -t_s$ with negative velocity $-v$ for $t < 0$, and instantly reversing its motion to velocity $+v$ for $t > 0$, finishing at the same position $x = vt_s$ at $t = t_s$; asymmetry in the PSF, therefore, may be expected. At 256 mm spiral field of view, an effective radial readout constant gradient strength g of 0.108 mT/m is used (calculated from the peak velocity phase shift of 41.9 rads for 1 m/second at the end of the 54.4 msec spiral readout, found at the edge of velocity *k* space for the constant angular rate spiral in Fig. 4), and $G = \gamma g$, as before. The velocity PSF $P(x)$ is obtained by the inverse FT of Equation 1:

$$P(x) = \mathrm{FT}^{-1}\left[(1 - H(t)) \exp(-i2\pi Gvt^2/2) + H(t) \exp(i2\pi Gvt^2/2)\right]. \quad [2]$$

Taking the inverse FT in Equation 2,

$$P(x) = \int_{-ts}^{0} \exp(-i2\pi Gvt^2/2) \exp(-i2\pi Gxt)\, dt + \int_{0}^{ts} \exp(i2\pi Gvt^2/2) \exp(-i2\pi Gxt)\, dt, \quad [3]$$

where t_s represents the edge of the spiral's coverage of *k* space, i.e., 54.4 msec, for the single-shot spiral example. Equation 3 simplifies to

$$P(x) = 2\cos(\pi Gx^2/v) \int_{-ts+x/v}^{x/v} \cos(\pi Gvu^2)\, du + 2\sin(\pi Gx^2/v) \int_{-ts+x/v}^{x/v} \sin(\pi Gvu^2)\, du. \quad [4]$$

Equation 4 was evaluated (20) by using the Fresnel integrals, giving a one-dimensional theoretical approximation (Fig. 5a) for the in-plane velocity PSF, which is real and shows asymmetry similar to that of the PSF phantom images (Fig. 1) and simulations (Fig. 4). The real only (i.e., signed magnitude, because the phase is constant and zero) calculated 1D-PSF (Fig. 5a) is consistent with a profile taken along the *x*-axis in a phase reconstruction (Fig. 5b) of the simulated 2D-PSF. The negative sign of some of the fringes in the leading edge supports the finding that the large, leading-edge fringe in the PSF phantom image (Fig. 5c) is in antiphase with the main part of the phantom, which is otherwise of uniform phase. However, the true PSF is two-dimensional because of the phase curvature along the k_y direction in the raw data, and no attempt is made to model this theoretically.

For interleaved spiral readouts, the phase curvature across the raw data due to in-plane motion is reduced by the shortened readout duration. In general, a quadratic reduction with gradient duration would be expected, but this is offset partially by an increase due to the slower spiral cycles used with more interleaves, and the phase curvature over velocity *k* space dropped by a factor of about 3 from 6-interleaf to 16-interleaf spiral imaging. For long moving objects in spiral imaging, distortion occurs mainly at the leading and trailing edges, which explains why the effect often is concealed when imaging in-plane flow, and this is also consistent with the raw data for such an object containing flow along *x* being significantly large only within the region $k_x \approx 0$ (Nishimura, personal communication). The small displacement and distortion perpendicular to the direction of motion (21) was not seen but could be estimated from the phase slope across the velocity

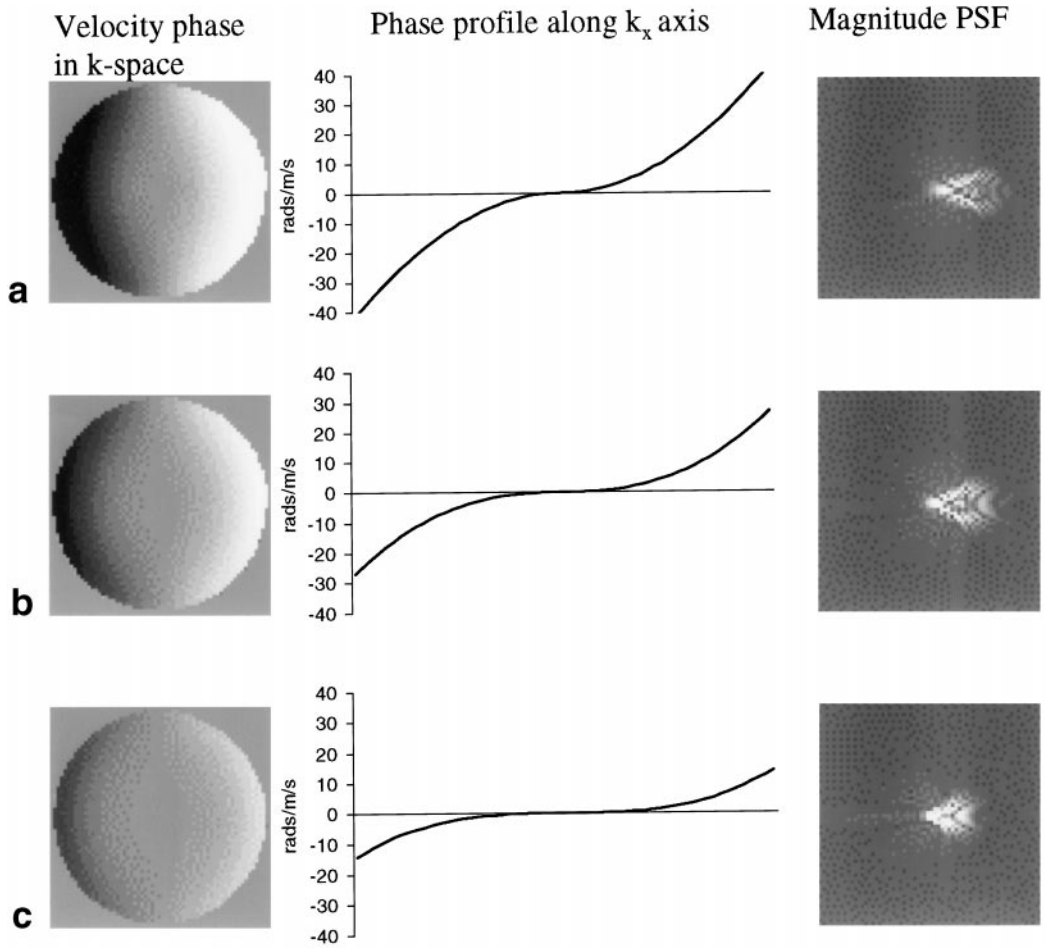

FIG. 4. **a:** Constant angular rate (CAR) spiral. **b:** Constant slew rate (CSR) spiral. **c:** Constant *k*-space speed (CKS) spiral. The left column shows velocity phase shift plotted over *k* space for velocity across the page from left to right during the spiral readout. The phase curvatures along k_x are shown in the centre column. Magnitude PSFs, which were obtained by using two-dimensional fast Fourier transform (2D-FFT) of the velocity phase shift in *k* space, are shown in the right column.

k-space plots (Fig. 4) in the direction perpendicular to the motion, which occurs because the zero crossings of the velocity phase sensitivity (12) are rotated slightly from the direction perpendicular to the direction of motion.

Single-Shot Imaging of Complex and Turbulent Flows

Single-shot spiral imaging gives no clear improvement in complex and turbulent flow signal uniformity compared with single-shot EPI with early coverage of central *k* space, although comparison is difficult because of different patterns of signal loss. Although the slice-selection gradient may cause some signal loss, this should be of a similar level and appearance in the two methods, because they used identical slice-selection waveforms. The results were surprising, because the early coverage of central *k* space before application of large in-plane gradients by spiral imaging should greatly reduce complex and turbulent flow signal loss. The term ''signal loss'' conventionally implies intravoxel phase dispersion due to flow-related phase shifts at central *k* space, but an additional mechanism of signal loss due to PSF distortion is now proposed to occur when the antiphase, leading-edge fringes in the spiral PSF overlap other in-phase signals. The PSF distortion effect is significant for the physiologic range of velocities only for imaging methods with a long *k*-space trajectory, and it is negligible in conventional imaging. PSF distortion also is irrelevant if conventional signal loss occurs, because there is no remaining signal to be distorted.

Complex Flow Signal Loss in Spiral Flow Imaging

Two computer simulations demonstrated how the distortion of in-plane flow may cause complex flow signal loss in spiral imaging. The first simulation approximates a situation that may occur when a skewed flow profile (for example, in curved flow) passes obliquely through the image plane (Fig. 6). A region of the signal excited by the slice-select pulse may have an in-plane component of velocity surrounded by regions of relatively stationary fluid.

For the single-shot spiral, 400 spins were simulated within a square block of 4 cm side length in the centre of the image. For 16-interleaf spiral imaging, 400 spins were simulated within a 2 cm-sided square block. Two experiments were calculated, one without motion (Fig. 7a,c) and one with the spins in the top right quarter of the square moving left at 50 cm/second (Fig. 7b,d). Where the leading edge of the moving signal overlaps the stationary signal, a reduction in signal occurs, and this is caused by the negative leading-edge fringe. The phase reconstructions show that the rest of the signal from the moving top right

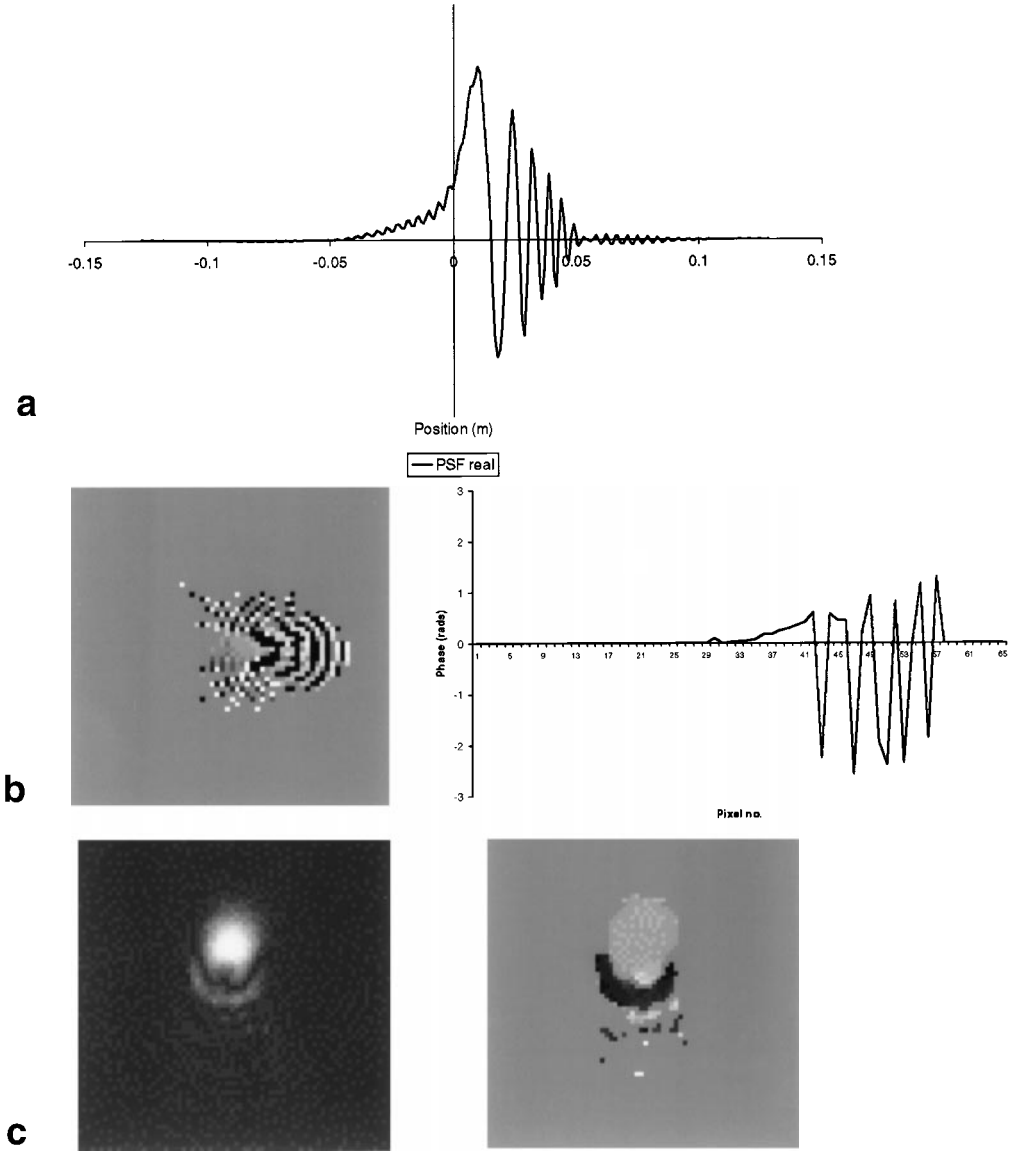

FIG. 5. **a:** Real part of the one-dimensional approximation to the in-plane motion spiral PSF. Imaginary part is zero. **b:** Phase reconstruction of the simulated PSF from Figure 4 and phase profile along the *x*-axis. The linear slope may be due to the image reconstruction's misalignment of central *k* space with the centre of the Fourier transform. **c:** Phase reconstruction of the six-interleaf spiral PSF phantom image from Figure 1.

quarter has *no* phase shift, confirming that the signal loss is not caused by the central *k*-space form of intravoxel phase dispersion. Some brightened regions of artefact also occur where in-phase moving signal overlaps the stationary signal.

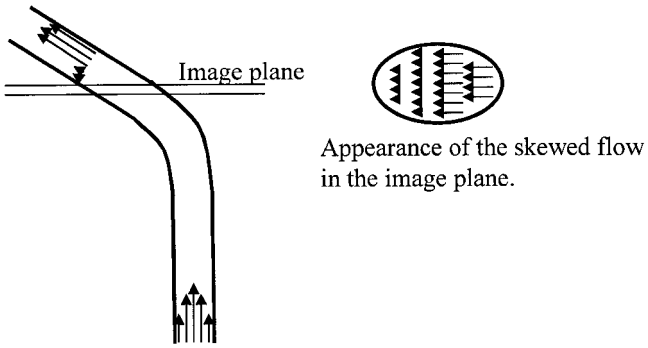

FIG. 6. Example of regions with differing in-plane flow velocity in complex flow.

The second simulation approximates the circulating flow imaged in the single-shot experiment. The central dark spot and segments of dark circular rings in the phantom image also occurred in a circulating flow model (Fig. 8), in which flow was converging toward the exit tube with a through-plane component (not shown). By using 1600 spins, a circular object of 40 mm radius was simulated, with circulating flow occupying a circular band between 10 mm and 20 mm radii. In this band, spins were simulated with a circulating and inward velocity at 45° to the tangent.

Two experiments were calculated, one without motion (Fig. 9a,c) and one with motion at 65 cm/second (Fig. 9b,d). The top row (Fig. 9b) shows the result of PSF distortion of the circulating band, and a central region of antiphase signal has appeared as well as the circular rings outside the 20 mm radius. When this is combined with spins outside the circulating band that are assumed to have relatively small in-plane velocity, regions of phase cancellation occur

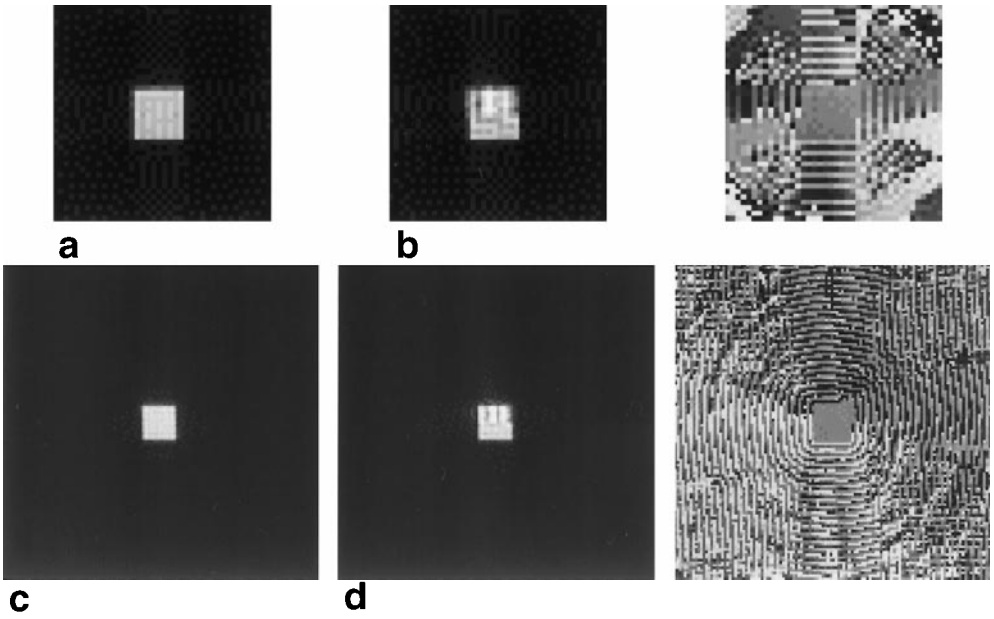

FIG. 7. Computer simulations of complex flow. **a,b:** Single shot spiral: static (a) and with top right quarter moving left (b; magnitude and phase). **c,d:** Sixteen-interleaf spiral: static (c) and with top right quarter moving left (d; magnitude and phase).

(Fig. 9d) that resemble the central dark spot and dark rings seen in the phantom image (Fig. 2d). Although this model may differ from the phantom flow, the simulation itself is not unreasonably extreme, and it shows signal loss due to complex flow in spiral imaging.

Turbulent Flow Signal Loss in Spiral Imaging

The effects of turbulent flow on rapid data acquisition during a long path in k space were shown in a random motion equivalent of velocity k space, using the random motion of a point source starting at the centre of the image plane at the time of the RF pulse. Parameters such as coherence time, peak velocity, randomness of direction, and degree of spatial coherence in the flow should be considered, and accurate simulation of any particular turbulent flow motion was not attempted. A coherence time of 1 msec was selected as an example of turbulent flow (22), with a range of peak velocities from 1 m/second to 5 m/second. A low-pass filter was applied to the random motion in order to approximate a 1 msec coherence time. Representing the randomly varying position as $f(t) = (f_x(t), f_y(t))$, the turbulence k-space map k_f was generated by

$$k_f(k_x, k_y) = 2\pi\gamma \int g_x(t)\, f_x(t)\, dt + 2\pi\gamma \int g_y(t)\, f_y(t)\, dt, \quad [5]$$

where $k_x = 2\pi\gamma \int g_x(t)\, dt$, and $k_y = 2\pi\gamma \int g_y(t)\, dt$.

The integrations were taken with $f(t) = 0$ and $t = 0$ at the time of the RF excitation. By taking the 2D-FFT of k_f, the distortion caused by random motion during the constant slew rate spiral (Table 1) was obtained. The distortion changes randomly with the phase shifts in k space, and the simulation is intended only to show the existence of the effect in spiral imaging rather than to reproduce any specific pattern of signal loss. Although the distortion caused by the random motion of the point source is shift invariant (i.e., the same distortion will occur if the same random motion is repeated starting anywhere in the image plane), in turbulent flow, the random motion itself will differ between points in the image plane. With increasing peak velocity, the distortion increased with an offset in the average direction of motion (Fig. 10). The main part of the brightest magnitude region remained in phase with the static image, but some pixels were in antiphase. The unchanged phase of the main part would be expected due to the absence of gradient waveforms before the acquisition of central k space, whereas the existence of some antiphase pixels also would be predicted from the in-plane motion effect demonstrated above.

In milder turbulence, it has been shown that large-scale structures may persist in the flow for times sufficiently long to be imaged by EPI velocity mapping (23), and these would lead to the more structured artefacts seen in the complex flow. This reflects the existence of a range of flow types from extreme turbulence with coherence times much shorter than single-shot imaging and spatial coherence much smaller than the image pixels to less turbulent flows with increasing temporal and spatial coherence that may be studied by single-shot imaging.

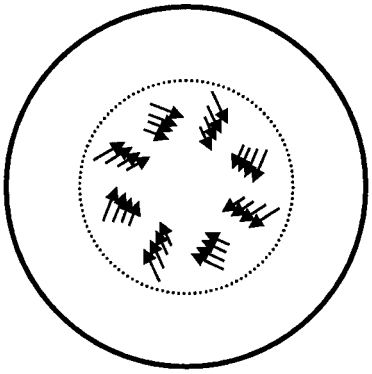

FIG. 8. Cross section of the circulating flow phantom showing the simulated motion.

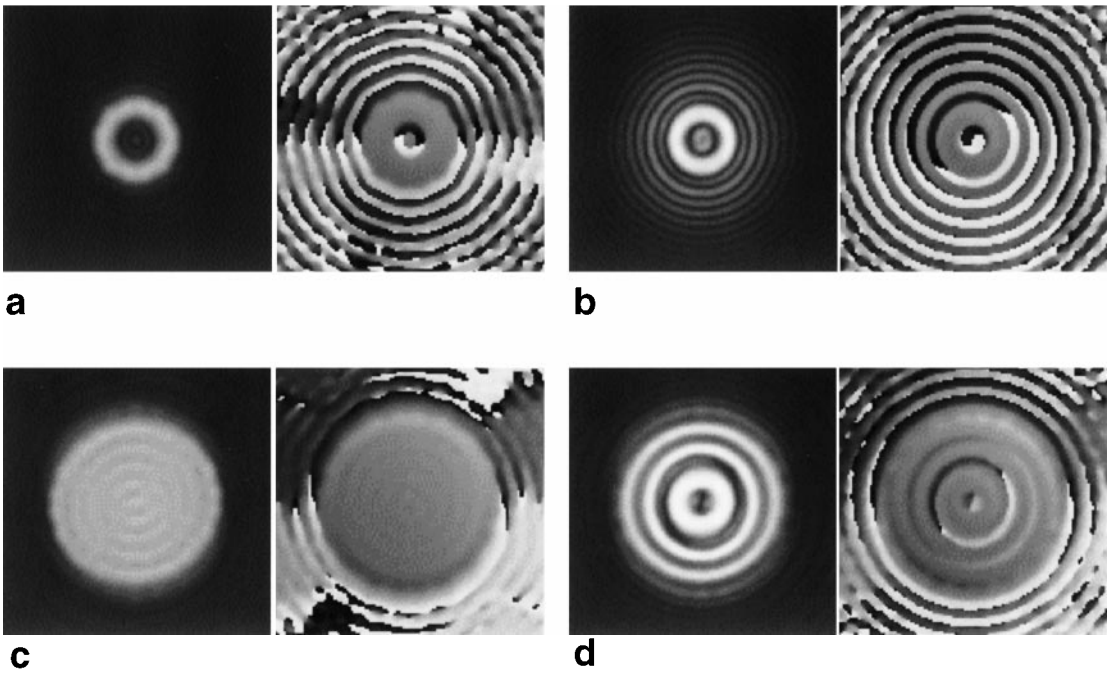

FIG. 9. Complex flow simulation in which single-shot spiral magnitude and phase images were reconstructed into a 256-pixel matrix (as in Fig. 2d). **a,b:** Circulating band of signal only: stationary (a) and at 65 cm/second (b). **c,d:** Circulating signal with static central and outer regions: stationary (c) and at 65 cm/second (d).

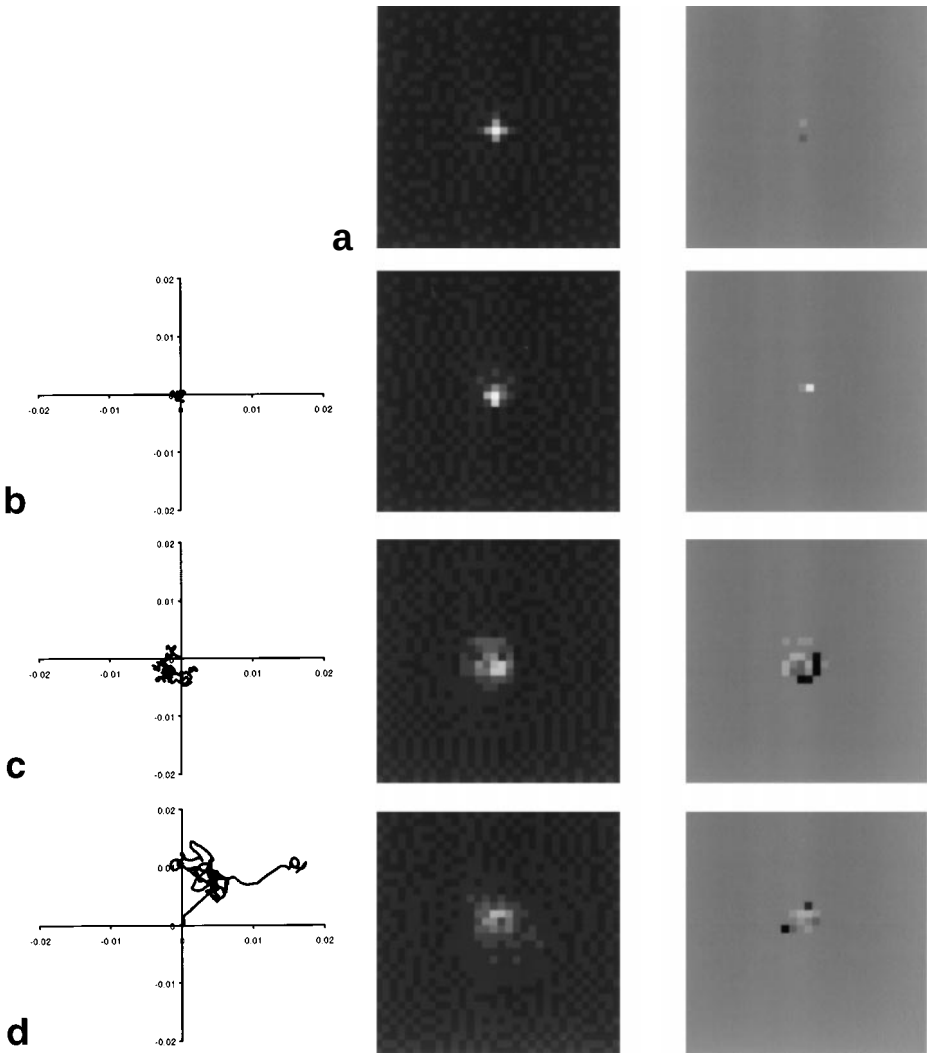

FIG. 10. Random-motion PSF distortion magnitude and phase images. **a:** Static. **b–d:** Peak speeds of 1 m/second, 3 m/second, and 5 m/second. The motion of the point source during the spiral readout is shown on the left (scale in metres). Phase images show only pixels with magnitudes that exceed 10% of the peak static PSF magnitude, and white and black pixels are in antiphase with the rest of the PSF in light grey.

CONCLUSIONS

The PSF distortion by in-plane motion during spiral imaging has been demonstrated in imaging, in simulations, and in theory. The PSF remains largely in phase with the static object, consistent with the reduction of intravoxel phase dispersive signal loss by the early acquisition of central *k* space. However, some of the pixels in the velocity PSF have the opposite phase, and it is proposed that these lead to a new mechanism of flow-related signal loss. For turbulent flow, the large, random phase variations toward the edges of *k* space cause distortion. The absence of large phase shifts in most of the random motion distortion is consistent with the absence of signal loss by the conventional intravoxel phase dispersion mechanism, but the distortion and the presence of antiphase pixels in it may cause signal loss in spiral imaging. Although the EPI PSF also is distorted, the effect is less relevant in EPI because of signal loss caused by phase dispersion at central *k* space. It appears that a robust method of single-shot flow imaging must have a short *k*-space path, and, for imaging of flow (but *not* of a moving point source) (24), even the segmented chirp effect is removed by using single-shot FLASH imaging. For the single-shot imaging of the highly complex or turbulent flows likely to occur in obstructed blood vessels, both EPI and spiral imaging may lose the flow signal for different reasons. The higher signal-to-noise ratio, shorter acquisition window, longer time available for velocity encoding (because it is not repeated for each spatial phase encoding), and flexibility with zonal imaging techniques of the EPI and spiral methods encourage their development, but flow effects must be monitored not only in EPI but also in spiral imaging.

REFERENCES

1. Nishimura DG, Irarrazabal P, Meyer CH. A velocity *k*-space analysis of flow effects in echo planar and spiral imaging. Magn Reson Med 1995;33:549–556.
2. Ljunggren S. A simple graphical representation of Fourier based imaging methods. J Magn Reson 1983;54:338–343.
3. Ahn CB, Kim JH, Cho ZH. High speed spiral scan echo planar imaging—I. IEEE Trans Med Imag 1986;5:2–7.
4. Blum MJ, Braun M, Rosenfeld D. Fast MRI using spiral trajectories. Austral Phys Eng Sci Med 1987;10:79–87.
5. Yudilevich E, Stark H. Spiral sampling in MRI-the effect of inhomogeneities. IEEE Trans Med Imag 1987;6:337–345.
6. Maeda A, Yokoyama T. Reducing chemical shift artefacts in MRI with time varying gradients. IEEE Trans Med Imag 1989;8:8–15.
7. Noll DC, Meyer CH, Pauly JM, Nishimura DG, Macovski A. A homogeneity correction method for MRI with time-varying gradients. IEEE Trans Med Imag 1991;10:629–637.
8. Noll DC, Pauly JM, Meyer CH, Nishimura DG, Macovski A. Deblurring for non-2D FT MRI. Magn Reson Med 1992;25:319–333.
9. Gatehouse PD, Firmin DN, Collins S, Longmore DB. Real time blood flow imaging by spiral scan phase velocity mapping. Magn Reson Med 1994;31:504–512.
10. Hardy CJ, Cline HE. Spatial localization in two dimensions using NMR designer pulses. J Magn Reson 1989;82:647–654.
11. Hardy CJ, Cline HE. Broadband NMR pulses with two-dimensional spatial selectivity. J Appl Phys 1989;66:1513–1516.
12. Meyer CH, Hu BS, Nishimura DG, Macovski A. Fast spiral coronary artery imaging. Magn Reson Med 1992;28:202–213.
13. Butts K, Riederer SJ. Analysis of flow effects in EPI. J Magn Reson Imag 1992;2:285–293.
14. Twieg DB, Katz J, Peshock RM. A general treatment of NMR imaging with chemical shift and motion. Magn Reson Med 1987;5:32–46.
15. Wedeen VJ, Wendt RE III, Jerosch-Herold M. Motional phase artefacts in Fourier transform MRI. Magn Reson Med 1989;11:114–120.
16. Jackson JI, Meyer CH, Nishimura DG, Macovski A. Selection of a convolution function for Fourier inversion using gridding. IEEE Trans Med Imag 1991;10:473–478.
17. Wiesmann F, Gatehouse PD, Panting JR, Taylor AM, Firmin DN, Pennell DJ. Comparison of fast spiral, echo planar and FLASH magnetic resonance imaging for cardiac volumetry at 0.5T. J Magn Res Img 1998;8:1033–1039.
18. Hardy CJ, Pearlman JD, Moore JR, Roemer PB, Cline HE. Rapid NMR cardiography with a half-echo M-mode method. J Comput Asst Tomogr 1991;15:868–874.
19. Crelier GR, Prussman KP, Boesiger P. Numerical simulation of 2D-selective excitation pulses in the presence of motion. In: Proceedings of the third annual meeting of the Society of Magnetic Resonance; 1995. p 1027.
20. Gatehouse PD. Rapid NMR imaging of blood flow [Ph.D. thesis]. London: University of London; 1998.
21. Groen JP, Kouwenhoven M, Van Muiswinkel A, Hofland L. Flow displacement artefacts in spiral imaging. In: Proceedings of the third annual meeting of the Society of Magnetic Resonance 1995. p 567.
22. Gatenby JC, Gore JC. Mapping of turbulent intensity by magnetic resonance imaging. J Magn Reson (B) 1994;104:119–126.
23. Kose K. One-shot velocity mapping using multiple spin-echo EPI and its application to turbulent flow. J Magn Reson 1991;92:631–635.
24. Matsuda T, Yamada H, Kida M, Sasayama S. Is 300ms too long for cardiac MRI? Feasibility study demonstrating changes in LV CS area with use of single-shot FLASH imaging. Radiology 1994;190:353–362.